Correlation-Enhanced Odd-Parity Interorbital Singlet Pairing in the Iron-Pnictide Superconductor LiFeAs

R. Nourafkan, G. Kotliar, and A.-M. S. Tremblay

Phys. Rev. Lett. **117**, 137001 — Published 20 September 2016

DOI: 10.1103/PhysRevLett.117.137001

Correlation-enhanced odd-parity inter-orbital singlet pairing in the iron-pnictide superconductor LiFeAs

R. Nourafkan[1], G. Kotliar[2], and A.-M.S. Tremblay[1,3]
[1]*Département de Physique and Regroupement québécois sur les matériaux de pointe, Université de Sherbrooke, Sherbrooke, Québec, Canada J1K 2R1*
[2]*Department of Physics & Astronomy, Rutgers University, Piscataway, NJ 08854-8019, USA and*
[3]*Quantum Materials Program, Canadian Institute for Advanced Research, Toronto, Ontario, M5G 1Z8, Canada*

The rich variety of iron-based superconductors and their complex electronic structure lead to a wide range of possibilities for gap symmetry and pairing components. Here we solve in the two-Fe Brillouin zone the full frequency-dependent linearized Eliashberg equations to investigate spin-fluctuations mediated Cooper pairing for LiFeAs . The magnetic excitations are calculated with the random phase approximation on a correlated electronic structure obtained with density functional theory and dynamical mean field theory. The interaction between electrons through Hund's coupling promotes both the intra-orbital $d_{xz(yz)}$ and the inter-orbital magnetic susceptibility. As a consequence, the leading pairing channel, conventional s^{+-}, acquires sizeable inter-orbital $d_{xy} - d_{xz(yz)}$ singlet pairing with odd parity under glide-plane symmetry. The combination of intra- and inter-orbital components makes the results consistent with available experiments on the angular dependence of the gaps observed on the different Fermi surfaces.

PACS numbers: 74.20.Pq, 74.70.Xa, 74.20.Rp

LiFeAs is a stoichiometric superconductor with superconducting $T_c \simeq 18$ K and no magnetic ordering. [1] Despite rather poor nesting [2–5], recent quasiparticle interference experiments identify the antiferromagnetic (AF) spin-fluctuation mediated mechanism as the predominant pairing interaction. [6] ARPES and quasiparticle-scattering interference measurements below T_c show that the superconducting (SC) gaps of LiFeAs are nodeless, with a Fermi surface (FS) dependence and a sizable variation along each FS. [2, 7, 8] Polarized neutron diffraction as a function of temperature has shown a suppression of the local spin susceptibility in the SC phase, suggesting singlet pairing. [9, 10]

In theoretical studies, the AF spin-fluctuation mediated pairing [11–14] and a combination of AF spin-fluctuation and orbital fluctuation mediated by phonons have been investigated. [15, 16] However, all studies are performed in the one-iron unit cell with various unfolding algorithms used to embed the correct symmetry. [17–21] This procedure is exact only for computing in-plane pairing. In addition, the SC gap equation is usually projected on the FS, the pairing interaction is symmetrized, [11] and the resulting equation is always solved in the BCS approximation. All of the above simplifications must be questioned before we can be confident of the results. Furthermore, for Fe-based superconductors (FeSCs) with a non-symmorphic point-group, [22] anti-symmetry of fermions does not place a constraint on the parity of the SC pairing channel. [23, 24] This allows for even-parity $d_{xz} - d_{yz}$ inter-orbital pairing [25], or for $d_{xy} - d_{xz(yz)}$ odd parity spin singlet pairing when there is orbital weight at the Fermi level from orbitals with different in-plane mirror reflection symmetry [26].

Hence, here we revisit spin-fluctuation mediated pairing by considering both Fe-$3d$ and As-$4p$ orbitals in the two-Fe unit cell. We solve the linearized Eliashberg equations [27] in the two-Fe Brillouin Zone (BZ) to investigate SC pairing and gap symmetry. Since there is increasing evidence that superconductivity does not emerge as a FS instability [40], we work in the orbital representation instead of projecting the gap equation on the FSs. Our results show that in the leading channel, with the conventional s^{+-} symmetry, odd parity inter-orbital pairing accompanies the usual intra-orbital pairing and increases with interactions, in particular with Hund's coupling. In contrast to previous studies [8, 11–13] we find that this state can reproduce the angular dependence of the gap on the electron pockets.

Electronic structure In LiFeAs, the bandwidth observed in ARPES is narrower than in LDA calculations and there are experimental evidences of long-lived magnetic moments. [9] This indicates the importance of correlations, so we employ the LDA+DMFT method to obtain the electronic structure. [41–43] Fig. 1 illustrates the LDA+DMFT partial spectral weight, $A_{ll}(\mathbf{k}, 0)$, of Fe t_{2g}- orbitals d_{xy} and $d_{xz,yz}$ on the FSs of LiFeAs. [44] The Fe e_g orbitals d_{z^2} and $d_{x^2-y^2}$ hybridize with As-p orbitals and contribute to the spectral weight lying above and below the Fermi level. The FS consists of three hole-like and two electron-like sheets around the center and corners of the BZ respectively. The two inner hole pockets are predominantly composed from d_{xz} and d_{yz} orbitals. The smallest hole pocket crosses the Fermi level only in close vicinity to the Γ point. It hybridizes with the d_{z^2} orbital near Z point and is closed there, while remaining $2D$ away from this point. The middle pocket has moderate k_z dispersion. The large hole-like Fermi surface originates purely from in-plane d_{xy} orbitals and therefore is $2D$ without noticeable k_z dispersion. The electron pockets are made from an admixture of d_{xy}, d_{xz} and d_{yz} orbitals. The electron pockets intersect at small k_z and their order flips, i.e., the inner pocket at $k_z = 0$ is the outer pocket at $k_z = \pi/c$.

Comparison to LDA, [27] shows that in LDA+DMFT: (a) The two inner hole pockets shrink while the outer one ex-

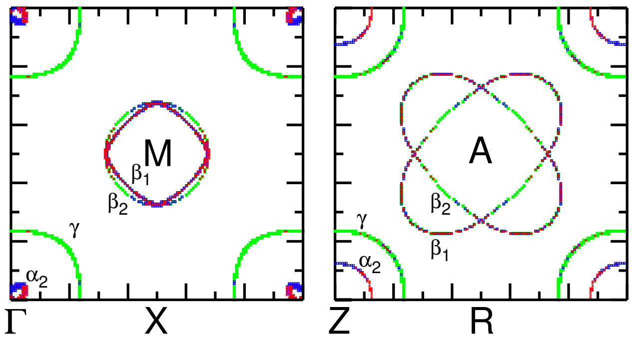

FIG. 1. (Color online) Partial spectral weight, $A_{ll}(\mathbf{k},0)$, of Fe t_{2g}- orbitals on the FS in the k_x-k_y plane with $k_z = 0$ (left), and $k_z = \pi/c$ (right) obtained from the LDA+DMFT calculation. Here the d_{xy}, d_{xz}, and d_{yz} orbitals are illustrated by green, blue and red colors, respectively. The α_1 pocket crosses the Fermi level only in close vicinity to the Γ point (not visible on this scale).

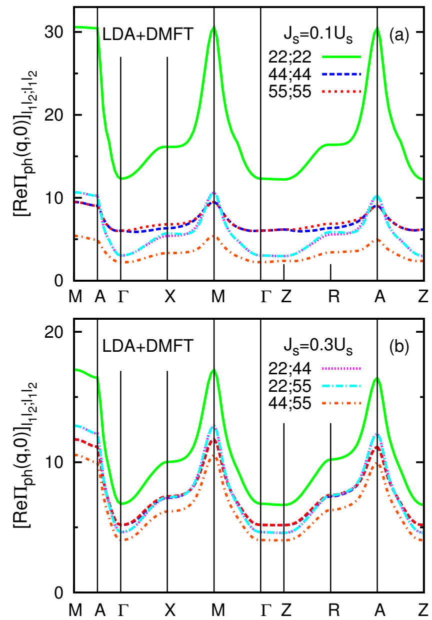

FIG. 2. (Color online) Several components of the pairing interaction of LiFeAs at $k_B T = 0.01$ eV in the particle-hole channel. There are two sets of screened interaction parameters yielding the same magnetic Stoner factor, namely $J_s = 0.1U_s$, $U_s = 2.4$ eV on the top and $J_s = 0.3U_s$, $U_s = 1.68$ eV on the bottom. The legend for the color coding is spread over both figures.

pands. (b) The middle hole pocket also deforms and takes on a butterfly shape at small k_z. [45] (c) At finite k_z, the outer hole-pocket acquires some d_{xz} and d_{yz} orbital weight in the direction of the A point. (d) The shrinkage of the two inner hole pockets leads to larger patches where d_{xz} and d_{yz} orbitals mix on these pockets. (e) The electron pockets are moderately expanded and they become closer to each other. [27]

The t_{2g} orbitals are the most strongly correlated [43, 45] as is apparent from the mass enhancements $m^*/m_{LDA} = 2.0$, 1.85, 3.13 and 2.7 for d_{z^2}, $d_{x^2-y^2}$, d_{xy}, and $d_{xz,yz}$ orbitals, respectively. The d_{xy} orbital has the strongest mass enhancement and shortest quasi-particle lifetime.

Effective pairing interaction A SC instability in the singlet channel occurs when the corresponding pairing susceptibility diverges as one lowers temperature. A divergent susceptibility signals the appearance of a pole in the corresponding reducible complex vertex function, which describes all scattering processes of two propagating particles. Using the Bethe-Salpeter equation, the condition for an instability is that an eignvalue of the matrix $-\mathbf{\Gamma}^{irr,s}\boldsymbol{\chi}^0_{pp}$ becomes unity. Here $\mathbf{\Gamma}^{irr,s}$ is the irreducible vertex function (effective pairing interaction) in the singlet channel, and $\boldsymbol{\chi}^0_{pp}$ is the bare susceptibility in the particle-particle (p-p) channel. [27, 46, 47]

The density/magnetic fluctuations contribute to the pairing interaction by entering the ladder vertex defined by $\mathbf{\Pi}_{ph} \equiv -(1/2)\mathbf{\Gamma}^{irr,d}\boldsymbol{\chi}^d_{ph}\mathbf{\Gamma}^{irr,d} + (3/2)\mathbf{\Gamma}^{irr,m}\boldsymbol{\chi}^m_{ph}\mathbf{\Gamma}^{irr,m}$ where $\boldsymbol{\chi}^{m(d)}_{ph}$ and $\mathbf{\Gamma}^{irr,m(d)}$ denote respectively the dressed susceptibility and the irreducible vertex function in the magnetic (density) channel. [27] These vertices can be calculated in the DMFT approximation. [48] However, such a calculation is prohibitively difficult for multiorbital systems at the low temperatures necessary to study superconductivity, [27] hence here we employ the random phase approximation (RPA). [49] In RPA, the irreducible vertex function is replaced by a static effective vertex which is parametrized by the *screened* intra-orbital Hubbard interaction, U_s, and the Hund's coupling J_s. [16, 27, 50, 51] The inter-orbital interaction and pair hopping are determined assuming spin-rotational symmetry. Note that even though the static effective vertices U_s and J_s capture Kanamori-Brückner screening effects, they do not fully capture the dynamics of screening. In particular, the RPA treatment misses the fact that at high fermionic frequencies one should recover the bare interactions.

Fig. 2 shows the pairing interaction, $\mathbf{\Pi}_{ph}$, at $k_B T = 0.01$ eV for two sets of screened interaction parameters that yield the same magnetic Stoner factor. [52] Here we only present the intra-sublattice components because the inter-sublattice components are relatively small. In what follows, we focus on the Fe-1 and Fe-2 (on A and B sublattices respectively) t_{2g} orbitals: d_{xy} will be referred as 2 (7) and d_{xz} and d_{yz} orbitals as 4 (9) and 5 (10). The dominant effective pairing interaction components are repulsive. As can be seen in Fig. 2(a), due to better nesting, the d_{xy} intra-orbital $(22;22)$ pairing vertex is dominant and the $d_{xz(yz)}$ intra-orbital $(44;44)$ is sub-dominant, yet on average it is larger than inter-orbital vertices $(22;44)$ and $(44;55)$.

However, at larger J_s/U_s the situation changes. For a fixed Stoner factor (proximity to magnetic transition) upon increasing the J_s/U_s ratio from Fig. 2(a) to Fig. 2(b), the d_{xy} intra-orbital pairing component decreases while the $d_{xz(yz)}$ intra-orbital components and the inter-orbital components increase slightly. This shows that a higher J_s, through coupling to the more correlated d_{xy} orbital, compensates the decrease of spin susceptibility expected from the lower U_s

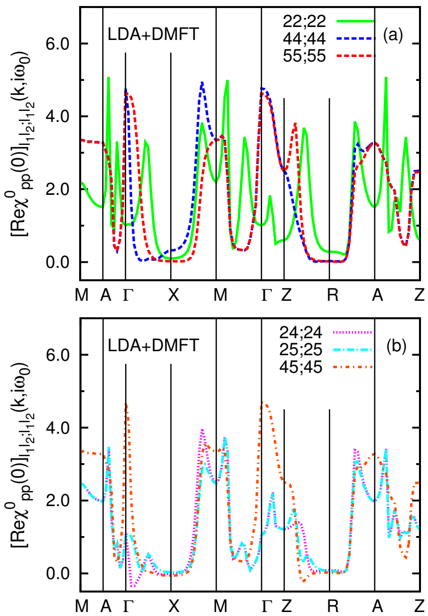

FIG. 3. (Color online) Real part of the several intra-sublattice components of the generalized particle-particle bare susceptibility at the lowest fermionic/bosonic Matsubara frequency.

(Fig. 2(b)). [27] Furthermore, since Hund's coupling correlates different orbitals, the inter-orbital components increase, becoming comparable with the $d_{xz(yz)}$ intra-orbital components. The d_{xy} intra-orbital vertex becomes less dominant at larger J_s/U_s. [53] This behavior of the magnetic susceptibility reflects itself directly in the pairing interaction (see supplemental material for the dressed susceptibilities in magnetic and charge channels).

Bare particle-particle susceptibility The generalized bare susceptibility in the p-p channel also enters the gap equation. [27] Fig. 3 shows the real part of several components of the generalized p-p bare susceptibility at the lowest fermionic/bosonic frequencies. The intra-orbital components are purely real. Both real and imaginary parts (see SM) show peaks at the position of FSs. For example, going from the Γ to the X point in the top panel, the three peaks are respectively related to the inner hole pocket with d_{xz} weight in close proximity to Γ, the middle pocket with d_{yz} weight and the outer pocket with d_{xy} weight. The peak heights are directly proportional to the corresponding orbital weight on the FSs and inversely proportional to the Fermi velocity. The peak widths are induced by correlation effects, implying that electrons near FSs may contribute to the Cooper pairing. In a non-interacting system the peak widths go to zero at zero temperature. [54] The larger $22;22$ peak component in the $M-\Gamma$ direction, compared with the $M-X(Y)$ direction, indicates that the SC gap on the outer electron pocket is larger in the $M-\Gamma$ direction.

In the BCS approximation, only real parts survive for the components considered here, due to a summation over Matsubara frequencies. In this case, the inter-orbital pairing is suppressed. Including the imaginary part in the full gap equation changes this trend. The imaginary parts of the inter-orbital components change sign between corner and center of the BZ. They have some symmetries that transfer to the gap function: (i) They are odd under exchange of orbital indices, (ii) There is also a π phase difference between the two Fe ions (see SM).

SC pairing symmetry in LDA+DMFT+RPA The leading pairing channel is a channel with dominant d_{xy}, d_{xz} and d_{yz} intra-orbital pairing. In our gauge, the gap function components have both real and imaginary part which satisfy $\mathrm{Re}\Delta_{ll}^{AA(BB)} = -\mathrm{Im}\Delta_{ll}^{AA(BB)}$. All intra-orbital components change sign between center and corner of the BZ (see Fig. 4), as expected in conventional s^{+-} pairing. The d_{xy} intra-orbital component dominates, but has a small value on the γ pocket. The d_{xz} and d_{yz} intra-orbital components are out of phase, i.e. $\Delta_{55}^{AA(BB)} \simeq -\Delta_{44}^{AA(BB)}$ (not shown). They take large values on the $\alpha_{1,2}$ hole pockets. The inter-sublattice components are much smaller than intra-sublattice ones, $\boldsymbol{\Delta}^{AA(BB)} >> \boldsymbol{\Delta}^{AB(BA)}$. The largest inter-sublattice component is Δ_{22}^{AB}. In orbital basis, the gap functions do not change much between $k_z = 0$ and $k_z = \pi/c$, hence we present only $k_z = 0$ results.

In agreement with the above pairing-interaction analysis, upon increasing J_s/U_s the $d_{xz/yz}$ intra-orbital pairing strengthen. Furthermore, the d_{xy}-d_{xz} and d_{xy}-d_{yz} inter-orbital pairings increase. Although they vary on a smaller interval, they are comparable with the $d_{xz/yz}$ intra-orbital components on the electron FSs (compare Fig. 4 top and bottom panels).

We verify that the gap function components of the leading channel satisfy the relations $\Delta_{l_1l_2}^{AA(BB)}(\mathbf{k}, i\omega_m) = \Delta_{l_1l_2}^{BB(AA)}(-\mathbf{k}, i\omega_m)$, and $\Delta_{l_1l_2}^{AA(BB)}(\mathbf{k}, i\omega_m) = \Delta_{l_2l_1}^{AA(BB)}(-\mathbf{k}, -i\omega_m)$. [56] The first relation says that the superconducting state does not break parity: In LiFeAs the inversion center is located in the middle of Fe-Fe link. Under parity operation the sublattice A maps to sublattice B and vice versa and $\mathbf{k} \to -\mathbf{k}$. The components of the gap function also satisfy the relation $\Delta_{l_1l_2}^{AA(BB)}(k_x, k_y, i\omega_m) = p_{l_1}p_{l_2}\Delta_{l_1l_2}^{BB(AA)}(k_x, k_y, i\omega_m)$, where p_l denotes the parity of orbital l with respect to in-plane mirror reflection symmetry. [57] This symmetry is defined by in-plane mirror reflection followed by a half-translation, expressed in units of the two-Fe unit cell, $\{\sigma^z|\frac{1}{2}\frac{1}{2}0\}$. Thus, the intra-orbital components on the two Fe are equal, while the inter-orbital components between one even-parity (d_{xy}) and one odd-parity (d_{xz}, d_{yz}) orbital, change sign between two Fe-ions. These components are the parity-odd under $\{\sigma^z|\frac{1}{2}\frac{1}{2}0\}$ spin singlet pairings. [26] Furthermore, as can be seen from Fig. 4, the in-plane intra-orbital components satisfy $\Delta_{ll}^{AA(BB)}(k_x, k_y) = \Delta_{ll}^{AA(BB)}(-k_x, -k_y)$, while the inter-orbital components between d_{xy} and $d_{xz(yz)}$ satisfy $\Delta_{l_1l_2}^{AA(BB)}(k_x, k_y) = -\Delta_{l_1l_2}^{AA(BB)}(-k_x, k_y)$ or $\Delta_{l_1l_2}^{AA(BB)}(k_x, k_y) = -\Delta_{l_1l_2}^{AA(BB)}(k_x, -k_y)$.

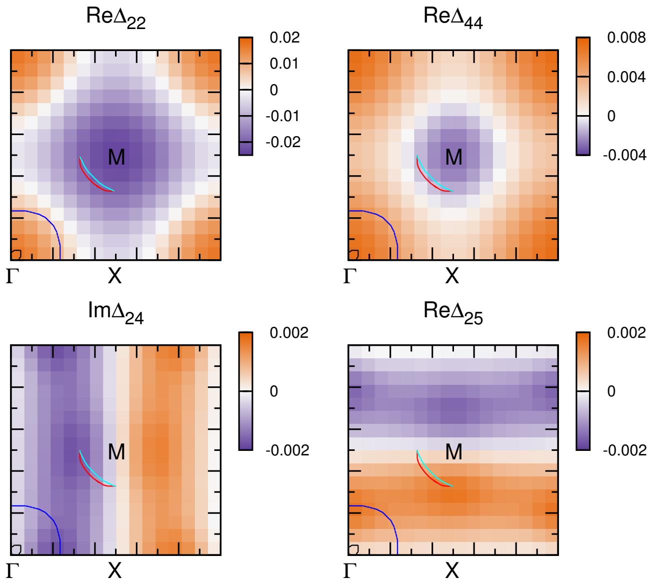

FIG. 4. (Color online) Top panels: The real part of the d_{xy} (left) and d_{xz} (right) in-plane intra-orbital components of the SC gap function at the lowest Matsubara frequency with largest eigenvalue in the orbital representation for $J_s/U_s = 0.3$ and $k_BT = 0.01$ eV. The imaginary part can be obtained from $\mathrm{Im}\Delta_{ll} = -\mathrm{Re}\Delta_{ll}$. Bottom panels: The real/imaginary part of the inter-orbital components of the SC gap function on sublattice A in the orbital representation, $\Delta^{AA}_{l_1 l_2}$. The corresponding components on sublattice B are out of phase with the displayed components, i.e. $\Delta^{BB}_{l_1 l_2} = -\Delta^{AA}_{l_1 l_2}$. The lines show one quarter of the Fermi surfaces.

Our calculations show that the gap symmetry of the leading channel is conventional s^{+-}. Indeed, although there is a phase difference between the d_{xz} and d_{yz} components of the gap function in the orbital basis, this phase difference is removed by another phase difference that arises when going to the Bloch basis corresponding to the $\alpha_{1,2}$ pockets. [27] In the *subleading* pairing channel, the d_{xy} intra-orbital component is in phase with d_{yz} and out of phase with d_{xz} intra-orbital components, which in the band representation gives s^{+-} gap symmetry with a sign change between $\alpha_{1,2}$ and γ pockets and between electron pockets and accidental nodes on the β_2 pocket. [14]

Finally, we comment on the SC gap magnitude on different FSs. [58] Diagonalizing the Bogoliubov quasi-particle Hamiltonian leads to a gap magnitude which has predominant $\cos 4\theta$ angular dependence on all pockets, as can be seen from Fig. 5. The angular dependence of the gap on the γ and of the average gap on the $\beta_{1,2}$ pockets are consistent with ARPES data: The gap is maximum at $\theta = 0, \pi/2$ and decreases when approaching $\theta = \pi/4$ (the direction toward M-point) on the γ pocket, while the average gap is maximum at $\theta = \pi/4$ (direction toward Γ-point) on the β pockets and decreases when approaching $\theta = 0, \pi/2$ where the two pockets cross. The gap on the β_2 electron pocket is increased in the direction of Γ-point due to a larger d_{xy} orbital content with a large pairing amplitude (see Fig. 4, upper panels). The gap on the β_1 electron pocket also shows a local enhancement at $\theta = \pi/4$. Due to interchange of electron pockets as a function of k_z, the gap on the inner pocket becomes larger than that on the outer pocket at a finite k_z. Hence, for these pockets, a direct comparison with ARPES data has to take averaging over a range of k_z into account. [59] The ratio between the average gap magnitude on β pockets and γ pocket is also consistent with ARPES results [7, 8]. However, the gap magnitude on the α pockets is not the largest. This discrepancy with ARPES results may come from the fact that ARPES is performed at very low temperature while the linearized Eliashberg gap equation is valid at temperatures infinitesimally close to the transition temperature. The tunneling spectroscopy study of LiFeAs has shown a temperature evolution of superconductivity. [60] A calculation at a lower temperature shows that the sharp peaks in the 44 and 55 bare paring susceptibilities, Fig. 3(a), grow faster than the wider peak for 22. This leads to an increase of the gap on the α pockets at lower temperatures.

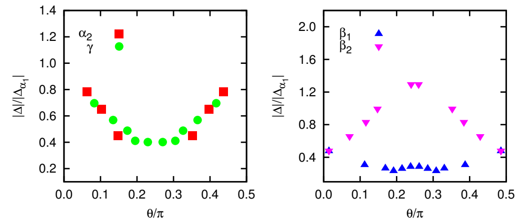

FIG. 5. (Color online) For $J_s/U_s = 0.3$, the SC gap magnitude (in units of the average gap magnitude on the α_1 pocket) as a function of the angle θ measured at the Γ and M points with respect to the x axis for $k_z = 0$ FSs.

Conclusion Solving the full linearized Eliashberg gap equation with both real and imaginary parts and including correlations in the LDA+DMFT framework leads to a detailed description of the leading pairing channel in LiFeAs. Accounting for correlations in the spin fluctuation approach allows to correctly capture not only nesting effects but also Fe-d orbital fluctuating moments with orbitally dependent dynamics. Although the intra-orbital d_{xy} spin susceptibility is dominant, Hund's coupling between orbitals on individual Fe atoms promotes both the intra-orbital $d_{xz(yz)}$ component and the inter-orbital d_{xy}-$d_{xz(yz)}$ components of the magnetic susceptibility. As a consequence, the leading paring channel, conventional s^{+-}, acquires inter-orbital singlet pairing component with odd parity under glide-plane symmetry. This type of pairing may also be realized in other iron-based superconductors. Antiphase s^{+-} pairing [14] is sub-leading. The combination of inter-orbital odd-parity and intra-orbital even parity singlet pairing leads to a description of the angle-dependence and of the relative magnitudes of the gap on the β and γ Fermi surfaces that is consistent with state of the art experiments.

R. N is deeply indebted to M. E. Pezzoli and F. Marsiglio for many insightful discussions. We thank K. Haule for his LDA+DMFT code and for discussions. R. N and A.-M.S. T are supported by the Natural Sciences and Engineering Research Council of Canada (NSERC) under grant RGPIN-2014-04584, and by the Tier I Canada Research Chair Program (A.-M.S.T.). G. K is supported by the NSF-DMR1308141. We acknowledge the hospitality of the CIFAR quantum materials program. Simulations were performed on computers provided by CFI, MELS, Calcul Québec and Compute Canada.

[1] J. H. Tapp, Z. Tang, B. Lv, K. Sasmal, B. Lorenz, P. C. W. Chu, and A. M. Guloy, Phys. Rev. B **78**, 060505 (2008).
[2] M. P. Allan, A. W. Rost, A. P. Mackenzie, Y. Xie, J. C. Davis, K. Kihou, C. H. Lee, A. Iyo, H. Eisaki, and T.-M. Chuang, Science **336**, 563 (2012).
[3] S. V. Borisenko, V. B. Zabolotnyy, D. V. Evtushinsky, T. K. Kim, I. V. Morozov, A. N. Yaresko, A. A. Kordyuk, G. Behr, A. Vasiliev, R. Follath, and B. Büchner, Phys. Rev. Lett. **105**, 067002 (2010).
[4] G. Lee, H. S. Ji, Y. Kim, C. Kim, K. Haule, G. Kotliar, B. Lee, S. Khim, K. H. Kim, K. S. Kim, K.-S. Kim, and J. H. Shim, Phys. Rev. Lett. **109**, 177001 (2012).
[5] P. M. R. Brydon, M. Daghofer, C. Timm, and J. van den Brink, Phys. Rev. B **83**, 060501 (2011).
[6] M. P. Allan, K. Lee, A. W. Rost, M. H. Fischer, F. Massee, K. Kihou, C.-H. Lee, A. Iyo, H. Eisaki, T.-M. Chuang, J. C. Davis, and E.-A. Kim, Nat. Phys. **11**, 177 (2015).
[7] K. Umezawa, Y. Li, H. Miao, K. Nakayama, Z.-H. Liu, P. Richard, T. Sato, J. B. He, D.-M. Wang, G. F. Chen, H. Ding, T. Takahashi, and S.-C. Wang, Phys. Rev. Lett. **108**, 037002 (2012).
[8] S. V. Borisenko, V. B. Zabolotnyy, A. A. Kordyuk, D. V. Evtushinsky, T. K. Kim, I. V. Morozov, R. Follath, and B. Bchner, Symmetry **4**, 251 (2012).
[9] J. D. Wright, M. J. Pitcher, W. Trevelyan-Thomas, T. Lancaster, P. J. Baker, F. L. Pratt, S. J. Clarke, and S. J. Blundell, Phys. Rev. B **88**, 060401 (2013).
[10] J. Brand, A. Stunault, S. Wurmehl, L. Harnagea, B. Büchner, M. Meven, and M. Braden, Phys. Rev. B **89**, 045141 (2014).
[11] Y. Wang, A. Kreisel, V. B. Zabolotnyy, S. V. Borisenko, B. Büchner, T. A. Maier, P. J. Hirschfeld, and D. J. Scalapino, Phys. Rev. B **88**, 174516 (2013).
[12] C. Platt, R. Thomale, and W. Hanke, Phys. Rev. B **84**, 235121 (2011).
[13] F. Ahn, I. Eremin, J. Knolle, V. B. Zabolotnyy, S. V. Borisenko, B. Büchner, and A. V. Chubukov, Phys. Rev. B **89**, 144513 (2014).
[14] Z. P. Yin, K. Haule, and G. Kotliar, Nat. Phys. **10**, 845 (2014).
[15] T. Saito, S. Onari, Y. Yamakawa, H. Kontani, S. V. Borisenko, and V. B. Zabolotnyy, Phys. Rev. B **90**, 035104 (2014).
[16] T. Yamada, J. Ishizuka, and Y. no, Journal of the Physical Society of Japan **83**, 043704 (2014).
[17] P. A. Lee and X.-G. Wen, Phys. Rev. B **78**, 144517 (2008).
[18] H. Eschrig and K. Koepernik, Phys. Rev. B **80**, 104503 (2009).
[19] O. Andersen and L. Boeri, Annalen der Physik **523**, 8 (2011).
[20] M. Casula and S. Sorella, Phys. Rev. B **88**, 155125 (2013).
[21] M. H. Fischer, New Journal of Physics **15**, 073006 (2013).
[22] V. Cvetkovic and O. Vafek, Phys. Rev. B **88**, 134510 (2013).
[23] J. Hu, Phys. Rev. X **3**, 031004 (2013).
[24] N. Hao and J. Hu, Phys. Rev. B **89**, 045144 (2014).
[25] T. Tzen Ong, P. Coleman, and J. Schmalian ArXiv e-prints (2014), arXiv:1410.3554.
[26] Y. Wang, T. Berlijn, P. J. Hirschfeld, D. J. Scalapino, and T. A. Maier, Phys. Rev. Lett. **114**, 107002 (2015).
[27] See supplemental material at [], which includes Refs. [28–39], for details of the electronic structure calculation, the spin fluctuation mediated pairing interaction and the RPA susceptibilities.
[28] S. Graser, T. A. Maier, P. J. Hirschfeld, and D. J. Scalapino, New Journal of Physics **11**, 025016 (2009).
[29] A. Toschi, A. A. Katanin, and K. Held, Phys. Rev. B **75**, 045118 (2007).
[30] G. Rohringer, A. Valli, and A. Toschi, Phys. Rev. B **86**, 125114 (2012).
[31] J. E. Hirsch and R. M. Fye, Phys. Rev. Lett. **56**, 2521 (1986).
[32] E. Gull, A. J. Millis, A. I. Lichtenstein, A. N. Rubtsov, M. Troyer, and P. Werner, Rev. Mod. Phys. **83**, 349 (2011).
[33] H. Hafermann, K. R. Patton, and P. Werner, Phys. Rev. B **85**, 205106 (2012).
[34] R. Yu, P. Goswami, Q. Si, P. Nikolic, and J. X. Zhu, Nat Commun **4**, 2783 (2013).
[35] J. Hu and H. Ding, Sci. Rep. **2**, 381 (2012).
[36] P. J. Hirschfeld, M. M. Korshunov, and I. I. Mazin, Reports on Progress in Physics **74**, 124508 (2011).
[37] T. Miyake, K. Nakamura, R. Arita, and M. Imada, Journal of the Physical Society of Japan **79**, 044705 (2010).
[38] T. Hajiri, T. Ito, R. Niwa, M. Matsunami, B. H. Min, Y. S. Kwon, and S. Kimura, Phys. Rev. B **85**, 094509 (2012).
[39] R. Nourafkan and A.-M. Tremblay, ArXiv e-prints (2016), arXiv:1601.05813.
[40] H. Miao, T. Qian, X. Shi, P. Richard, T. K. Kim, M. Hoesch, L. Y. Xing, X.-C. Wang, C.-Q. Jin, J.-P. Hu, and H. Ding, Nat Commun **6**, 7056 (2015).
[41] M. Aichhorn, L. Pourovskii, V. Vildosola, M. Ferrero, O. Parcollet, T. Miyake, A. Georges, and S. Biermann, Phys. Rev. B **80**, 085101 (2009).
[42] K. Haule, C.-H. Yee, and K. Kim, Phys. Rev. B **81**, 195107 (2010).
[43] Z. P. Yin, K. Haule, and G. Kotliar, Nat. Mater. **10**, 932 (2011).
[44] To keep a minimum variation of orbital content within a pocket, the electron pockets are chosen as inner and outer pockets β_1 and β_2 rather than as two crossed ellipse-like pockets of equal size.
[45] J. Ferber, K. Foyevtsova, R. Valentí, and H. O. Jeschke, Phys. Rev. B **85**, 094505 (2012).
[46] N. E. Bickers, "Self-consistent many-body theory for condensed matter systems," (Springer-Verlag, New York, 2004) Chap. 6, pp. 237–296.
[47] G. Esirgen and N. E. Bickers, Phys. Rev. B **57**, 5376 (1998).
[48] A. Toschi, R. Arita, P. Hansmann, G. Sangiovanni, and K. Held, Phys. Rev. B **86**, 064411 (2012).
[49] T. A. Maier, M. Jarrell, and D. J. Scalapino, Phys. Rev. B **75**, 134519 (2007).
[50] Y. Yanagi, Y. Yamakawa, and Y. Ōno, Phys. Rev. B **81**, 054518 (2010).
[51] H. Miyahara, R. Arita, and H. Ikeda, Phys. Rev. B **87**, 045113 (2013).
[52] The distance from magnetic and charge/orbital fluctuation criticality is determined by the corresponding (dimensionless) magnetic (density) Stoner factor $\alpha_{\mathbf{q}}^{m(d)}$, which is the largest eigenvalue of $\mathbf{\Gamma}^{irr,m}\chi^0_{ph}(\mathbf{q}, i\nu_n = 0)$ $(-\mathbf{\Gamma}^{irr,d}\chi^0_{ph}(\mathbf{q}, i\nu_n = 0))$.
[53] The $22;44$ $(44;55)$ components in the magnetic and charge susceptibilities in the p-h channel are related to the $24;42$ and

$42; 42$ ($45; 54$ and $54; 54$) components of the pairing interaction in the p-p channel.
[54] R. Nourafkan, Phys. Rev. B **93**, 241116 (2016).
[55] See Eq.[S33] in the supplementary material [27].
[56] The combination of these relations gives $\Delta_{l_1 l_2}^{AA(BB)}(\mathbf{k}, i\omega_m) = \Delta_{l_2 l_1}^{BB(AA)}(\mathbf{k}, -i\omega_m)$.
[57] The five Fe $3d$ orbitals can be categorized into even orbital parity (d_{3z^2}, $d_{x^2-y^2}$, d_{xy}) with $p_l = +1$ and odd orbital parity (d_{xz}, d_{yz}) with $p_l = -1$.
[58] The linearized Eliashberg gap equation only gives gap symmetry, not gap magnitude. But to make contact with experiment one can approximately extract the relative size of the gaps on the different FSs. This can be done by defining a Bogoliubov quasi-particle Hamiltonian including the real part of the self-energy at the Fermi level in the normal part, and employing the gap function obtained from the gap equation as an estimate of the anomalous self-energy. [14] After diagonalizing the Bogoliubov quasi-particle Hamiltonian, the gap magnitude at momentum $\mathbf{k}$ is given by half of the difference between the smallest positive eigenvalue and the largest negative eigenvalue. This is the quasi-particle gap which reduces to the SC gap on the FSs. For this calculation, the gap function on a very dense $\mathbf{k}$-mesh is required. Since the gap function is a smooth function, its magnitude on a denser mesh can be obtained by spline interpolation.
[59] S. Borisenko, D. Evtushinsky, I. Morozov, S. Wurmehl, B. Bchner, A. Yaresko, T. Kim, M. Hoesch, T. Wolf, and N. Zhigadlo, "Direct observation of spin-orbit coupling in iron-based superconductors," (2014), arXiv:1409.8669.
[60] P. T. Nag, R. Schlegel,D. Baumann,H.-J Grafe,R. Beck,S. Wurmehl,B. Buchner, and C. Hess ArXiv e-prints (2015), arXiv:1509.03431.